Applied Thermal Engineering 239 (2024) 122153

Contents lists available at ScienceDirect

Applied Thermal Engineering

journal homepage: www.elsevier.com/locate/apthermeng

Research Paper

The effect of nucleating agent on the multiphase change materials for energy storage in buildings

Rizal Sinaga [a,b,*], Jo Darkwa [a], Mark Worall [a], Weiguang Su [c,d]

[a] Buildings, Energy and Environment Research Group, The Faculty of Engineering, The University of Nottingham, University Park, Nottingham NG7 2RD, UK
[b] Engineering Management Study Program, Institut Teknologi Del, Laguboti, Toba Samosir 22381, Indonesia
[c] School of Mechanical Engineering, Qilu University of Technology (Shandong Academy of Sciences), 3501 Daxue Road, Jinan 250353, China
[d] Shandong Institute of Mechanical Design and Research, 250031, Jinan, China

ARTICLE INFO

Keywords:
Multiphase change material
Nucleating agent
Microencapsulation
Thermal energy storage
Phase change material

ABSTRACT

Phase change materials (PCMs) have the potential to be used for widespread energy storage applications in buildings. However, available PCMs can only function at fixed phase transitional temperatures, restricting their seasonal applicability. To this end, some studies have been carried out to develop multiphase change materials (MCMs). Prior to having competitive advantage, their encapsulation efficiency needs to be improved. In this study, MCM has been developed by combining two microencapsulated PCMs (MEPCMs), through Van der Wall's interaction forces phenomenon. In-situ polymerisation was adopted to fabricate the MEPCMs by employing RT22 and RT64 as PCMs. The optimal amount of nucleating agent played a crucial role in obtaining high encapsulation efficiencies of microencapsulated RT22 (MERT22) and RT64 (MERT64) by 90.43% and 84.07%, respectively. The developed MCM achieved melting temperatures at 23.01 °C and 56.64 °C, with combined energy storage capacity of 163.17 J/g, and encapsulation efficiency of 83.81%. The MCM also had thermal stability temperature of 142.71 °C, exceeding common building operating temperature. The nucleating agent also affected the sample morphology and particle size distribution, which therefore requires optimisation. There is also the need for thermal enhancement since it remains as one of the limiting factors of PCMs.

1. Introduction

Thermal energy contributes a considerable proportion of the energy consumed in many regions worldwide and has a significant influence in the emission of greenhouse gases [1]. The building sector accounts for approximately 40% of the total global energy consumption [2] with the bulk proportion being used for space heating/cooling and hot water supply. Furthermore, the expected growth of roughly 2 billion in the world's population over the next two decades means that there will be a greater demand for new buildings, which will in turn increase energy consumption [3]. There is therefore, the need for energy efficient technologies for minimising energy consumption and greenhouse gas emissions in the buildings sector.

Phase change materials (PCMs) have been identified as potential energy storage materials for reducing energy consumption in buildings [4–7]. For instance, Darkwa [8] and Zhou et al. [9] were able to achieve as much as 30% reduction in heating and cooling loads in a building with composite PCM drywall systems. Other studies [10–12] did also achieve similar encouraging results by incorporating PCM into building envelopes under different climatic conditions. Apart from integrating PCMs into building fabrics, Fazilati and Alemrajabi [13], Sharif et al. [14], and Najafian et al. [15] were able to shift peak cooling and heating loads with PCMs into hot water storage systems. Murray and Groulx [16] and Delgado et al. [17] also achieved 34% and 44% increases in thermal capacities respectively with PCMs for domestic hot water storage systems.

However, commercially available PCMs are only able to function at fixed phase transition temperatures thus limiting their flexibility for simultaneous heating and cooling or seasonal applications in buildings. For example in a building where both heating and cooling are required throughout the year, these PCMs cannot be utilised for that dual function since they have single phase transition temperature. Similarly in hot water storage systems, these PCMs have a limitation based on the fact that when water temperature exceeds the single phase transition

* Corresponding author at: Buildings, Energy and Environment Research Group, The Faculty of Engineering, The University of Nottingham, University Park, Nottingham NG7 2RD, UK.
E-mail addresses: rizal.sinaga@nottingham.ac.uk, rizal.sinaga@del.ac.id (R. Sinaga).

https://doi.org/10.1016/j.applthermaleng.2023.122153
Received 27 September 2023; Received in revised form 28 November 2023; Accepted 30 November 2023
Available online 3 December 2023

Table 1
Materials for the fabrication of MERT22 and MERT64.

Items		Sample A (1503)		Sample B (3101)		Sample C (1403)	
		MERT22-A	MERT64-A	MERT22-B	MERT64-B	MERT22-C	MERT64-C
O/W emulsion	**RT22 (g)**	10	–	10	–	10	–
	RT64 (g)	–	10	–	10	–	10
	Nano-silicon dioxide (g)	1.2	1.2	1.2	1.2	1.2	1.2
PPS	**Melamine (g)**	2.0	2.0	2.0	2.0	2.0	2.0
	Formaldehyde 36% (g)	3.2	3.2	3.2	3.2	3.2	3.2
Nucleating agent	**Ammonium chloride (g)**	0	0	0.125	0.125	0.25	0.25

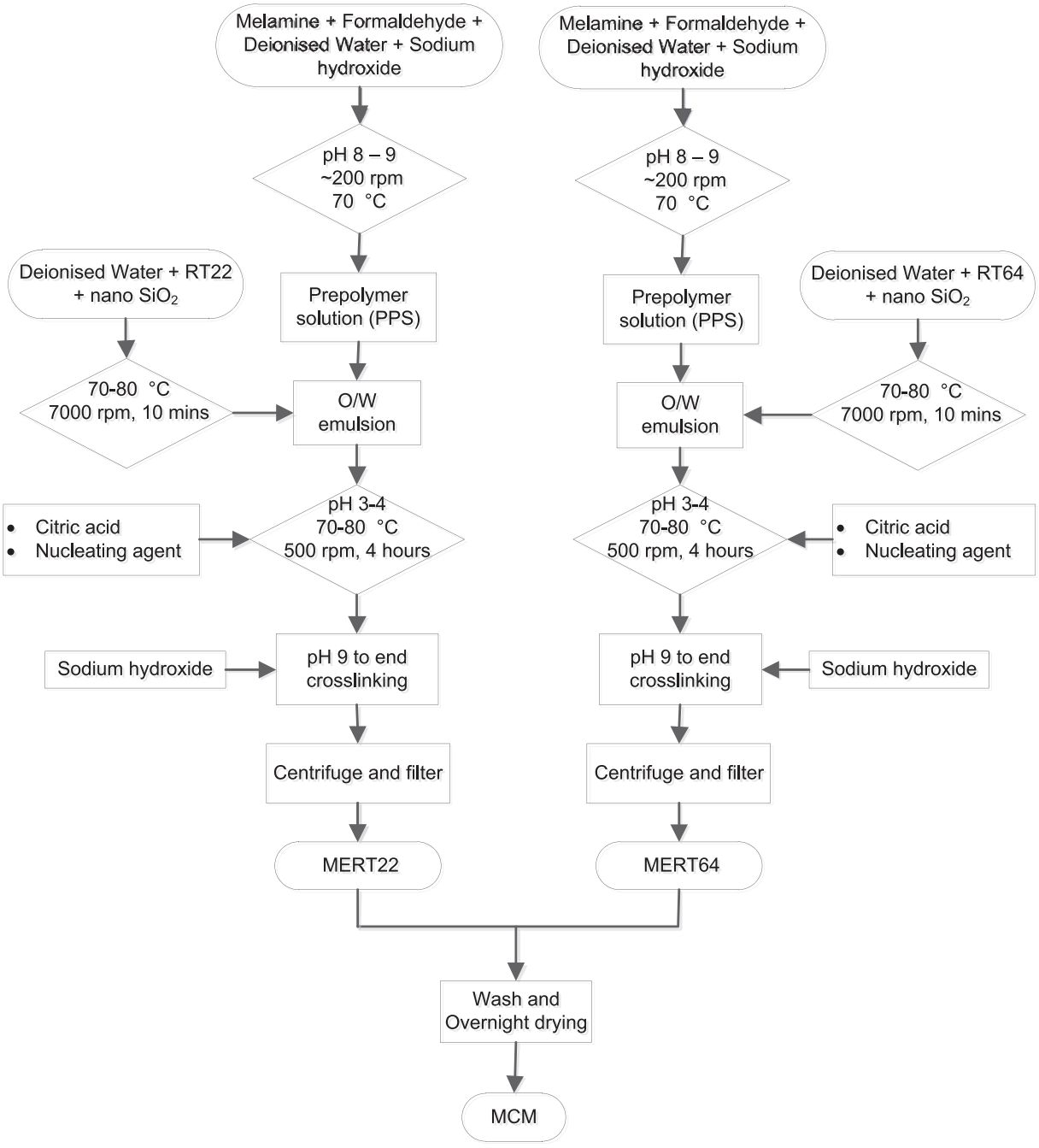

Fig. 1. The fabrication procedure of MCM.

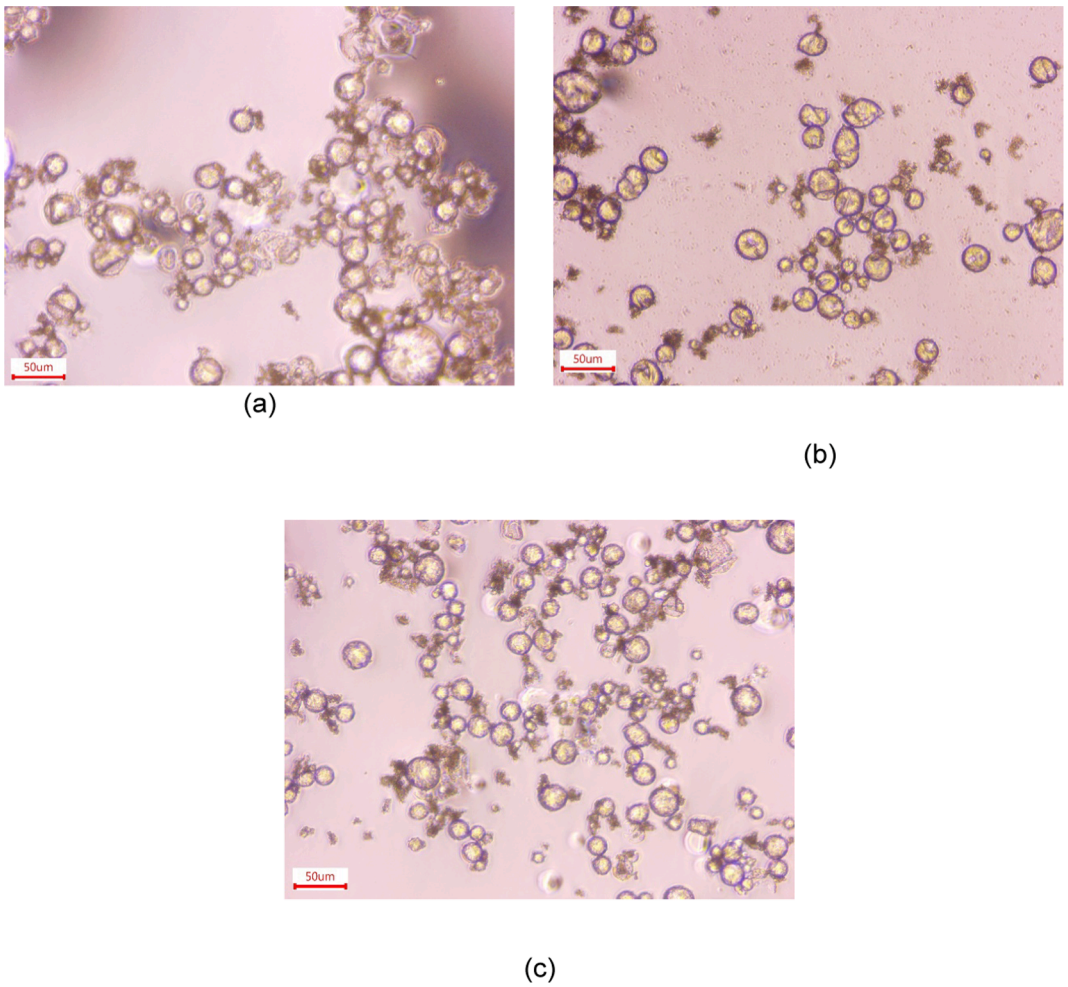

Fig. 2. Microscopic images of MEPCM slurries (a) MERT22-A, (b) MERT22-B, and (c) MERT22-C.

temperatures of the PCMs, water becomes the main storage medium because of its high sensible heat capacity. The hot water systems are therefore unable to fully benefit from the high thermal storage capacity of the PCMs.

To this end, different mixtures of binary PCMs have been investigated. For instance, Bo et al. [18] investigated the thermal properties of binary mixtures consisting of hexadecane and tetradecane at various volume ratios but achieved unsatisfactory results. Ma et al. [19] combined octadecane and butyl stearate with various acrylate-based copolymer shells could not achieve multiple phase transition temperatures. Further study by Li et al. [20] based on investigating multiple fatty acids consisting of capric acid, lauric acid, palmitic acid, and tearic acid. They attained a phase transition temperature between 19.1 and 53.2 °C but the sample was not encapsulated.

The encapsulation method is developed to retain physico-chemical characteristics of core material during extensive exposure to external conditions [21,22], such as leakage protection during the phase transition of PCMs. Moreover, the recent progress in micro and nanotechnology has resulted in the extensive utilisation of energy storage materials in various specifc fields [23] by selecting appropriate shell material [24]. Therefore, the microencapsulated phase change materials (MEPCMs) have the potential to be integrated into several construction materials typically employed in building application, including cements [25], gypsum wallboard [26], and plasterboard [27]. Nevertheless, it should be noted that all the integrated MEPCMs are limited to functioning at a single phase transition temperature.

There are few studies on the development of multiphase change materials (MCMs) with multiple transitional temperatures by adopting microencapsulation technique. For instance, Graham et al. [28] microencapsulated magnesium nitrate hexahydrate and sodium sulphate decahydrate in poly(ethyl-2-cyanoacrylate) (PECA) shell material through in-situ inverse miniemulsion polymerisation method. The results showed multiple melting points at 32–33 °C and 93–97 °C, but with maximum latent heat reduction of about 80–83%. Yang et al. [29] produced microencapsulated compound by mixing polyethylene glycol (PEG)800 and PEG1000 in a polyurethane shell through interfacial polymerisation method. They obtained multiple melting temperatures at 23.12/ 32.88 °C and 28.02/ 36.24 °C during storage and discharging processes, respectively. Darkwa and Su [30] and Su et al. [31] also developed a novel MCM by combining two MEPCMs in poly(melamine formaldehyde) (PMF) shell through in-situ polymerisation process and achieved multiple melting temperatures of 23.4 °C/34.5 °C. Nevertheless, there was reduction of 6.3%−11.4% in the energy storage capacity as compared with the average value of the MEPCMs, which was attributed to the encapsulation efficiency of the capsules. These outcomes clearly show some limitations in terms of encapsulation efficiency and operating temperature range.

Nucleating agents have been identified as important ingredients for ensuring good thermal stability and reduction of supercooling in MEPCMs [32,33]. For instance, Alvarado et al. [34] microencapsulated n-tetradecane with silica and tetradecanol as the nucleating agents. The results showed that 0.2 wt% silica had no effect on the supercooling of MEPCM. On the other hand, supercooling could be effectively reduced when MEPCM was combined with 2% or 4% tetradecanol. Magnetic particles are also known as nucleating agent owing to their capacity to absorb electromagnetic radiation [35], hence potentially offering

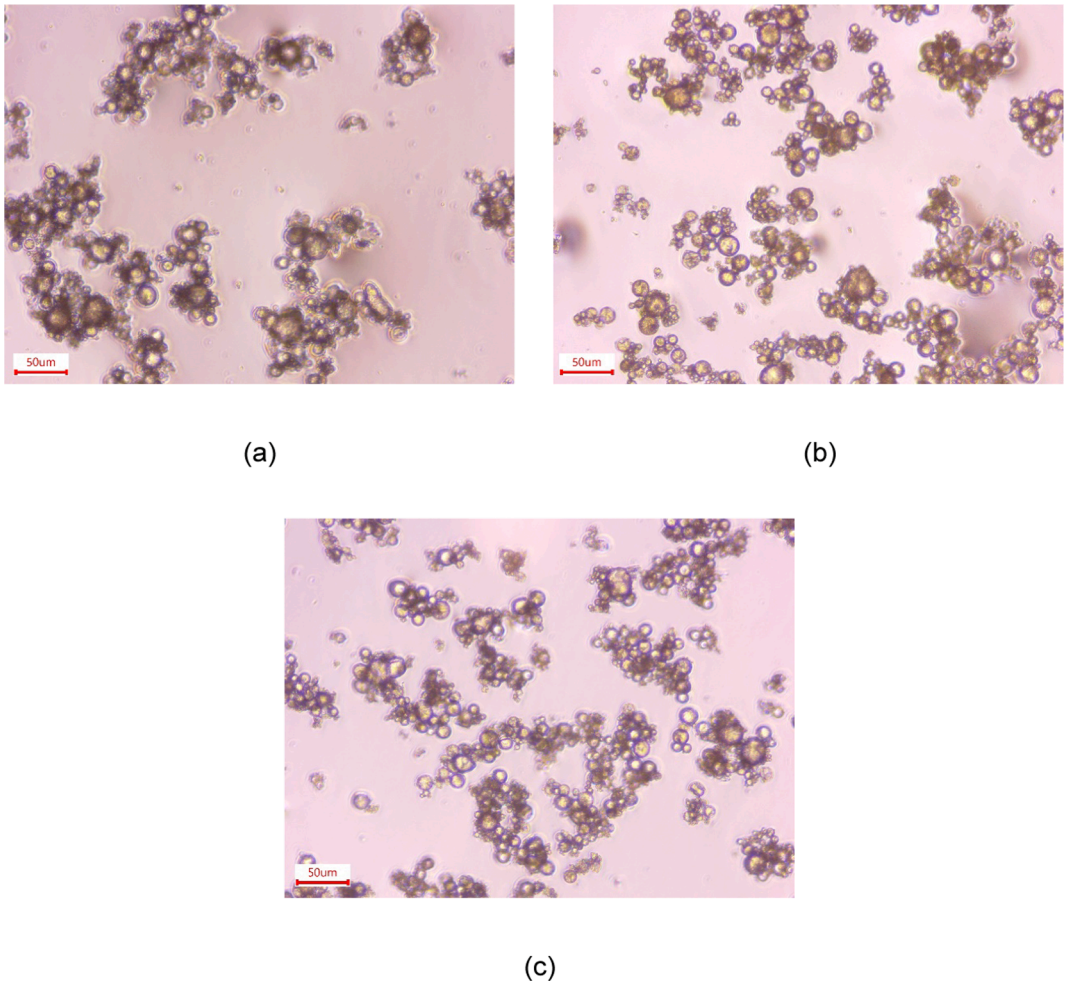

Fig. 3. Microscopic images of MEPCM slurries (a) MERT64-A, (b) MERT64-B, and (c) MERT64-C.

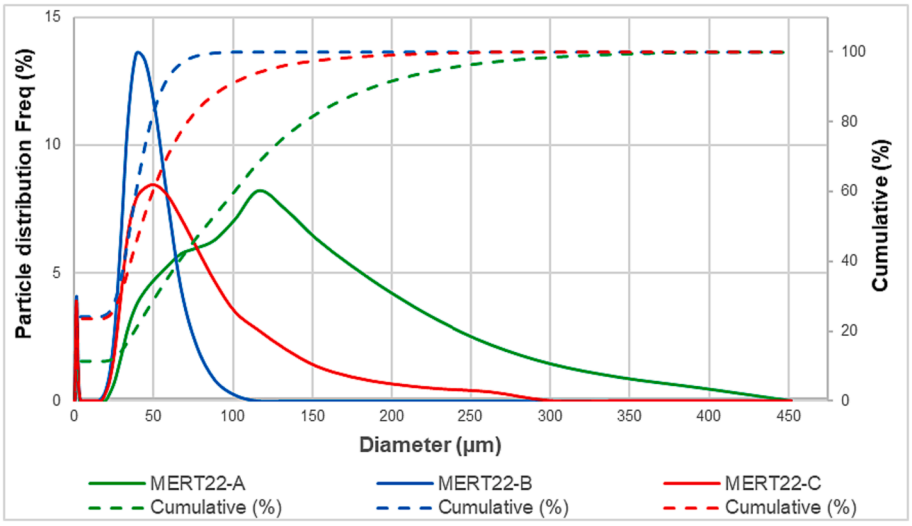

Fig. 4. PSD of MERT22 samples.

innovative enhancements to the performance of MEPCMs. For instance, Lashgari [36] microencapsulated n-Hexadecane in poly(methyl methacrylate) (PMMA) shell through suspension polymerisation with Fe_3O_4 magnetic nanoparticles as nucleating agent. The results showed a reduction of 41.6% in supercooling with 4 wt% of nucleating agent compared to the samples without nucleating agent. It was also reported that the addition of Fe_3O_4 nanoparticles had no significant effect on the morphology of the MEPCMs.

According to number of studies [37–41], ammonium chloride appears to be an effective nucleating agent, but the appropriate amount

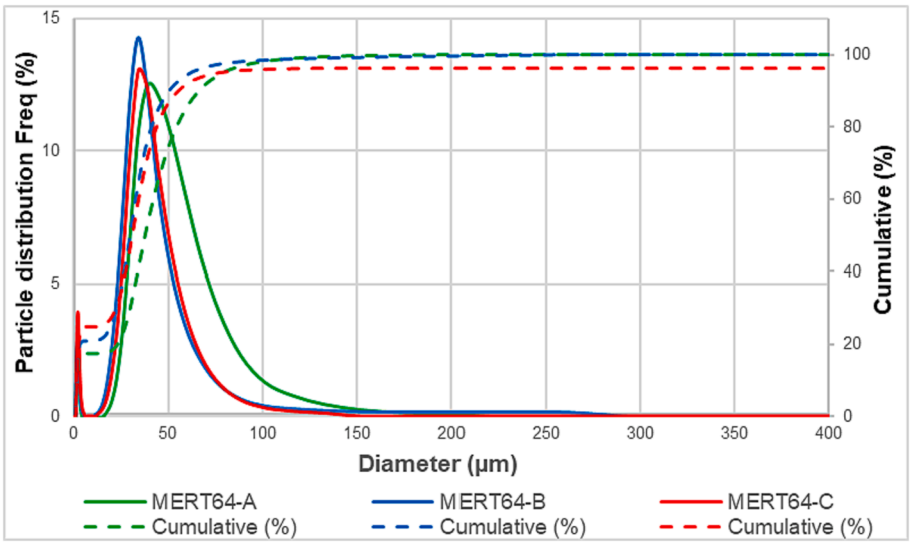

Fig. 5. PSD of MERT64 samples.

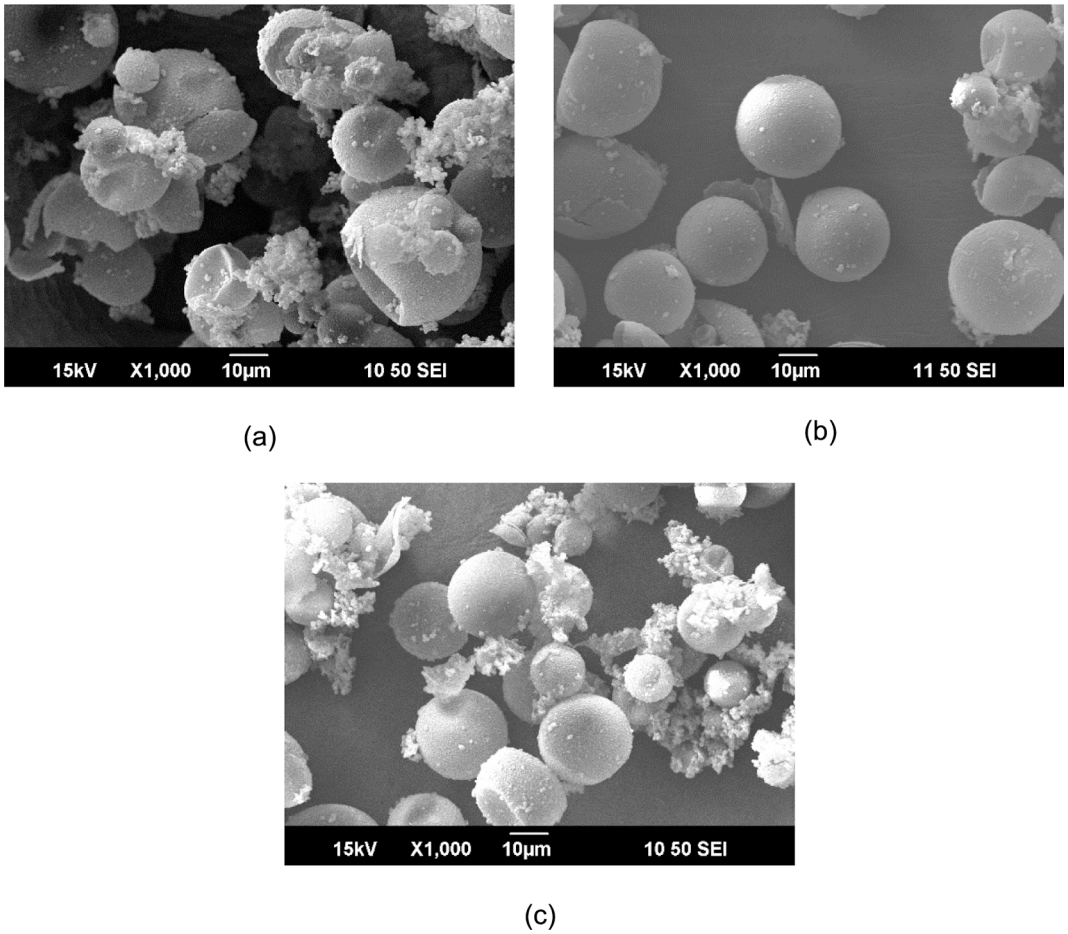

Fig. 6. SEM images of (a) MERT22-A, (b) MERT22-B, and (c) MERT22-C.

needs to be established for each encapsulation process. For instance, Li et al. [42] fabricated MEPCMs by in situ polymerisation method with 5.4 g of ammonium chloride and was able to significantly enhance thermal stability and reduce supercooling. In general, the thermal performance of MEPCMs depends largely on the content of the core materials and proportion of nucleating agents. The above studies have clearly highlighted most of the crucial factors influencing the successful development of good-quality MCM. This study was therefore focused on investigating the optimal quantity of ammonium chloride as nucleating agent for the development of MCM with much wider operating temperature range than currently available.

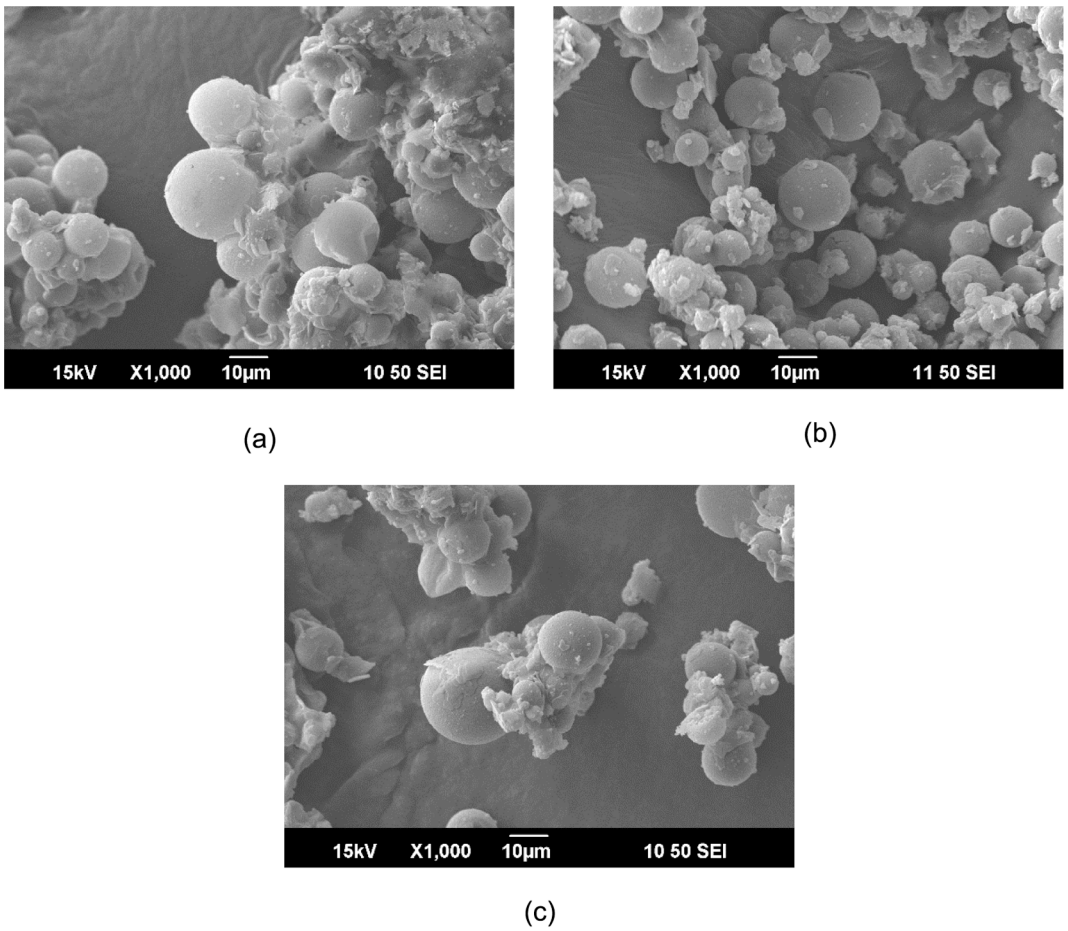

Fig. 7. SEM images of (a) MERT64-A, (b) MERT64-B, and (c) MERT64-C.

2. Development of MCM

The approach was based on firstly encapsulating two types of paraffins (RT22 and RT64) in PMF shell before combining them through van der Waal's interaction force to obtain the MCM samples. The samples were then characterised to establish their thermophysical and structural properties.

2.1. Materials

Rubitherm® RT22 and RT64 were selected as core materials with melting temperature of about 22 °C and 64 °C, respectively. Melamine (99% purity) and formaldehyde (36% purity) were obtained from Sigma Aldrich and VWR BDH Chemicals, respectively, and used as shell monomer. Nanosilicone dioxide hydrosol was prepared and used as an emulsifier. Sodium hydroxide and citric acid were used for modifying the pH levels of the solutions, which were supplied respectively by VWR BDH Chemicals and Fisher Scientific. Ammonium chloride (GPR Rectapur) was selected for nucleating agent and supplied by VWR BDH Chemicals. Ammonium chloride was added to the solution at various weight proportions to produce three MEPCM samples each for microencapsulated RT22 (MERT22) and microencapsulated RT64 (MERT64) as presented in Table 1.

2.2. Fabrication of MEPCM and MCM

Fig. 1 shows that 10 g of PCM sample was initially mixed with 140 g of deionised water, followed by 1.2 g of nano-silicon dioxide to produce the oil/water (O/W) emulsion. The O/W emulsion was subsequently stirred with a digital disperser at a speed of 7,000 rpm for about 10 min to obtain a uniform mixture. The next step was to prepare the prepolymer solution (PPS) by mixing 2 g of melamine and 3.2 g of formaldehyde in 10–15 ml of deionised water. Sodium hydroxide solution (0.2 wt %) was also added to the solution to maintain a pH value of 9 and then stirred at 200 rpm in a water bath until it became clear. The PPS was then combined with the O/W emulsion and heated up in a water bath to a temperature of 70–80 °C. After this process, 10 wt% of citric acid solution was employed to reduce the pH to about 3–4 before the crosslinking process started, folllowed by the addition of nucleating agent at different weights as shown in Table 1. The stirring speed of solution was subsequently reduced to 500 rpm over a period of 4 h in a water bath at a temperature of 80 °C. To terminate the crosslinking, 5 wt% of sodium hydroxide solution was utilised to increase the pH value to 9. Each sample was further centrifuged at 2,000 rpm for 5 min before the top layers were collected, filtered, and washed with deionised water at temperature of 80 °C to obtain the MEPCM samples. Finally, 50 wt% of each MECPM samples was combined in a beaker glass filled with deionised water and then mixed at a speed of 200 rpm for 10 min, before drying them overnight in an oven at a temperature of 80 °C to obtain the MCM samples.

3. Results and analysis

3.1. Characterisations of microencapsulated PCM (MEPCM)

3.1.1. Microscopy analysis

OPTIKA Microscope IM-3 was used to view and evaluate the slurry sample structure during the production process. During the fabrication process, each of the three MEPCMs samples were collected in slurry form to observe their microstructure. As shown in Fig. 2(a), sample MERT22-

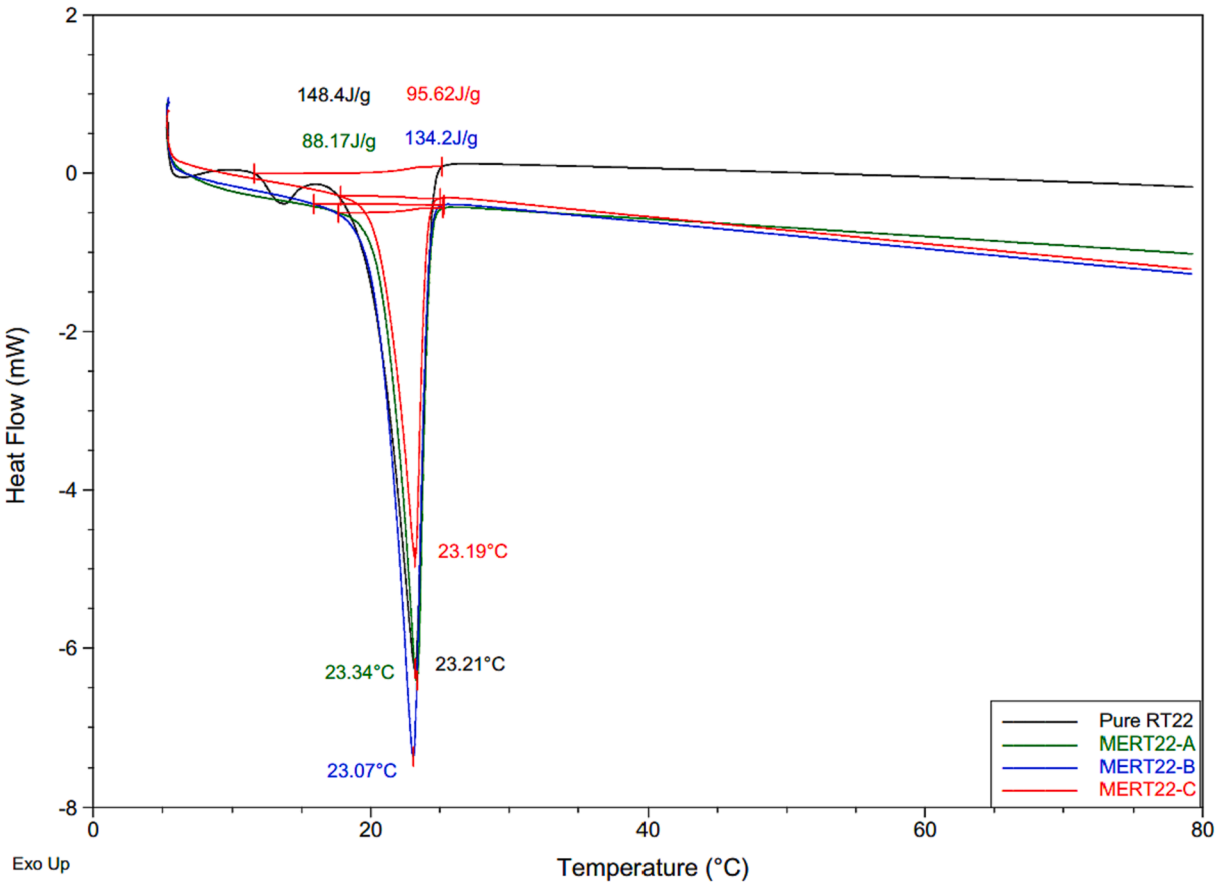

Fig. 8. DSC profile of pure RT22 and MERT22.

A, (which does not contain any nucleating agent), exhibited more irregular shapes and deformation than the other samples. This result is consistent with other findings [43,44] that emphasised the significance of nucleating agents in microencapsulation. However, the right amount of nucleating agent is necessary for achieving high encapsulation efficiency for MEPCMs. This can be seen by comparing the other two samples, where MERT22-B appears to contain less damage and residue than MERT22-C.

Fig. 3 depicts the microscopic images of the MERT64 samples. Similar to MERT22, the sample without nucleating agent in Fig. 3(a), showed more irregular particles. It is also clear that more residues can be observed in MERT64-C than in MERT64-B sample, which is attributed to the relatively larger amount of nucleating agent used. Due to the nature of these structures, the resulting diameter distribution can also be larger than predicted [45].

3.1.2. Particle size distribution

The particle size and distribution of sample were analysed by using HORIBA LA 960. The sample was dispersed in distilled water in a fraction cell. It is required the refractive index and the absorption of the substance to calculate the size of the microcapsule. In this regard, the refractive index of PMF was chosen as 1.3755 [46].

The results of the particle size distribution (PSD) analysis of the MERT22 samples are presented in Fig. 4. The analysis shows that sample MERT22-B, which contains 0.125 g of nucleating agent, achieved the narrowest particle size distribution profiling with an average diameter of 32.43 μm. The mean particle size of MERT22-C was larger than that of MERT22-B at 47.33 μm, which was attributed to the residue shown in the microscopic image. Sample MERT22-A did display the widest distribution profile with mean particle size of 94.48 μm. This is evidenced by the irregular shape and fractured shells shown in the microscopic image which would ultimately lead to agglomeration.

Fig. 5 shows the PSD results for the MERT64 samples and similar to MERT22-B, sample MERT64-B which contains 0.125 g of nucleating agent displayed the narrowest particle distribution profile and the smallest particle size diameter among all the MERT64 samples. The mean particle size was obtained by 30.16 μm, as compared with 38.50 μm and 56.71 μm for MERT64-A and MERT64-C, respectively. The results have demonstrated the importance of establishing the appropriate amount of nucleating agent for the development of the microcapsules.

3.1.3. Scanning electron microscope (SEM) evaluation

The surface morphologies of the samples were observed by means of scanning electron microscope (SEM) utilising JEOL 6490LV. The instrument was utilised in a high-vacuum configuration with an acceleration voltage of 15 kV, accompanied by the implementation of a secondary electron detector. Due to the non-conductive nature of the shell material, the samples were initially coated with gold layer to improve their electrical conductivity prior to microscopic inspection [47].

Fig. 6 shows the SEM images for all the MERT22 samples. It can be observed that the samples without the appropriate quantity of nucleating agent sustained greater amount broken shells and irregular shapes. For instance, sample MERT22-A, which did not contain any nucleating agent at all suffered the greatest damage. Meanwhile, a lot of nanoparticles and residues were observed on the surface of sample MERT22-C in Fig. 6(c), which contained more nucleating agent than MERT22-B. This is attributed to the fact that with the release of more ammonia gas in the nucleating agent, more hydrogen chloride is produced in the water solution, thus resulting in a decrease in pH value which leads to accelerated cross-linking [42,48]. On the other hand, MERT22-B with just adequate amount of nucleating agent, achieved the best morphology

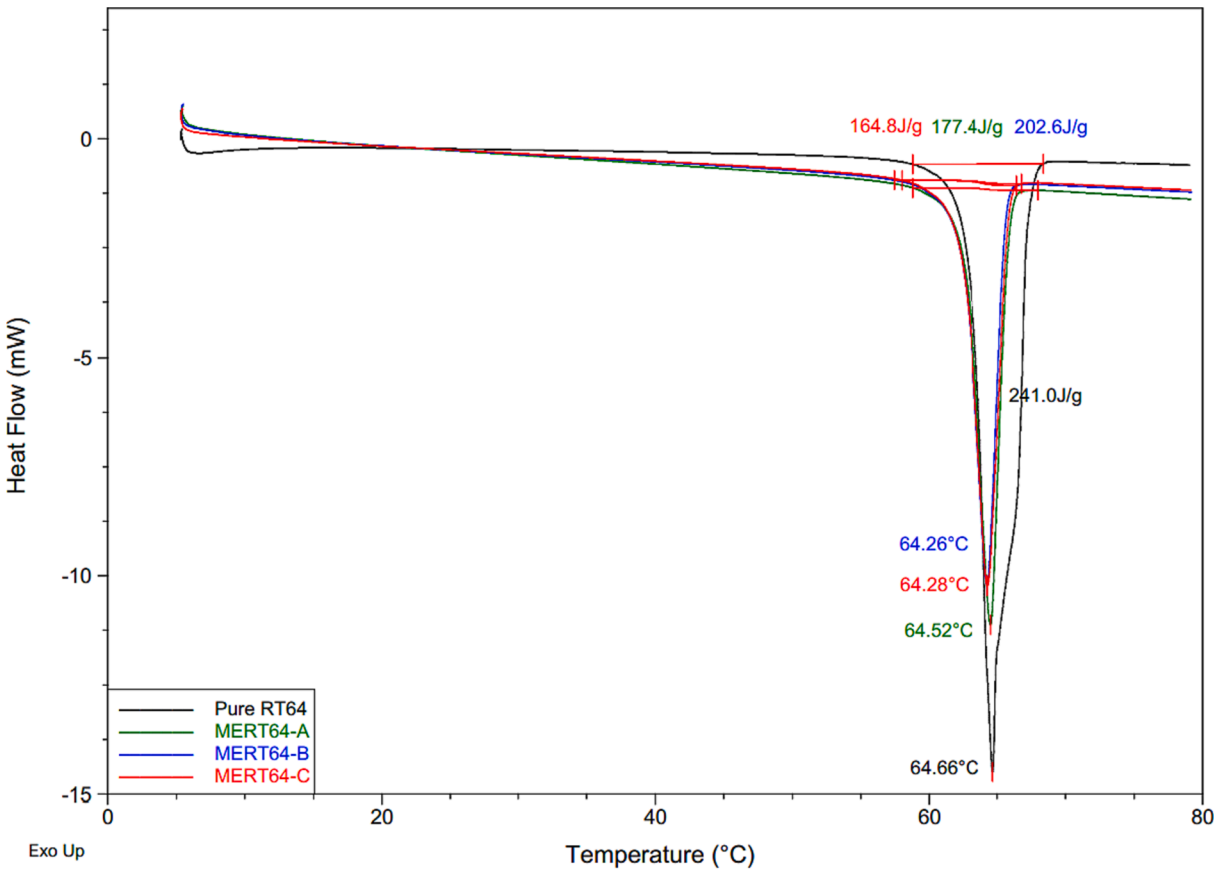

Fig. 9. DSC profile of pure RT64 and MERT64.

Table 2
Thermophysical properties of tested samples.

Samples	Melting temperature (°C)	Latent heat (J/g)	EE (%)	Stability temperature (°C)
RT22	23.21	148.4	–	106.85
MERT22-A	23.34	88.17	59.41	128.99
MERT22-B	23.07	134.2	90.43	129.21
MERT22-C	23.19	95.62	64.43	129.03
RT64	64.66	241	–	184.16
MERT64-A	64.52	177.4	73.61	186.09
MERT64-B	64.26	202.6	84.07	200.53
MERT64-C	64.28	164.8	68.38	190.89

with more regular shapes, smooth surfaces, and less nanoparticle residue.

The results for the MERT64 samples are also presented in Fig. 7. As in the case of MERT22, the sample without (MERT64-A) and with more nucleating agent (MERT64-C) suffered the greatest damage in terms of shell deformation and excessive residues. These findings are in agreement with the microscopic images in Fig. 3.

3.1.4. Energy storage capacity

The enthalpies of fusion and melting temperatures of all samples were determined by differential scanning calorimetric (DSC) technique using TA Instruments DSC Q2000 equipment. Using nitrogen as a purge gas, the samples were analysed at atmospheric pressure at a rate of 2 °C/min from 5 to 80 °C.

Fig. 8 shows the DSC test results for the pure RT22 and MERT22 samples. It can clearly be seen that the melting temperatures of the MERT22 samples were fairly close to that of pure RT22 at 23 °C. However, their latent heat capacities were significantly reduced by about 9.57% until 40.59%. The DSC test results for the pure RT64 and MERT64 samples are presented in Fig. 9 showing identical peak melting temperatures of about 64 °C. As found for the MERT22 samples, their latent heat capacities were much reduced within a range of 15.93% and 31.62%.

Based on the latent heat values, the encapsulation efficiencies (EE) of all the samples were determined by using the formula:

$$EE(\%) = \frac{\Delta h_{m,MEPCM}}{\Delta h_{m,PCM}} \times 100\% \quad (1)$$

where $\Delta h_{m,MEPCM}$ and $\Delta h_{m,PCM}$ denote the latent heat of MEPCM and pristine PCM, respectively.

As summarised in Table 2, MERT22-B and MERT64-B samples achieved the highest encapsulation efficiencies of 90.43% and 84.07 %, respectively, with less reductions in their corresponding latent heat capacities.

3.1.5. Thermal stability

Thermogravimetric (TG) analysis was carried out on the samples to determine their thermal stabilities using TA Instruments TGA Q500. This was achieved under nitrogen gas protection by observing the weight changes of the samples as a function of rising temperatures from 40 to 500 °C and at a heating rate of 10 °C/min.

The result for RT22 and MERT22 samples are presented in Fig. 10. The thermal stabilities of the MERT22 samples were found to be identical until weight loss started at about 129 °C. The thermographic

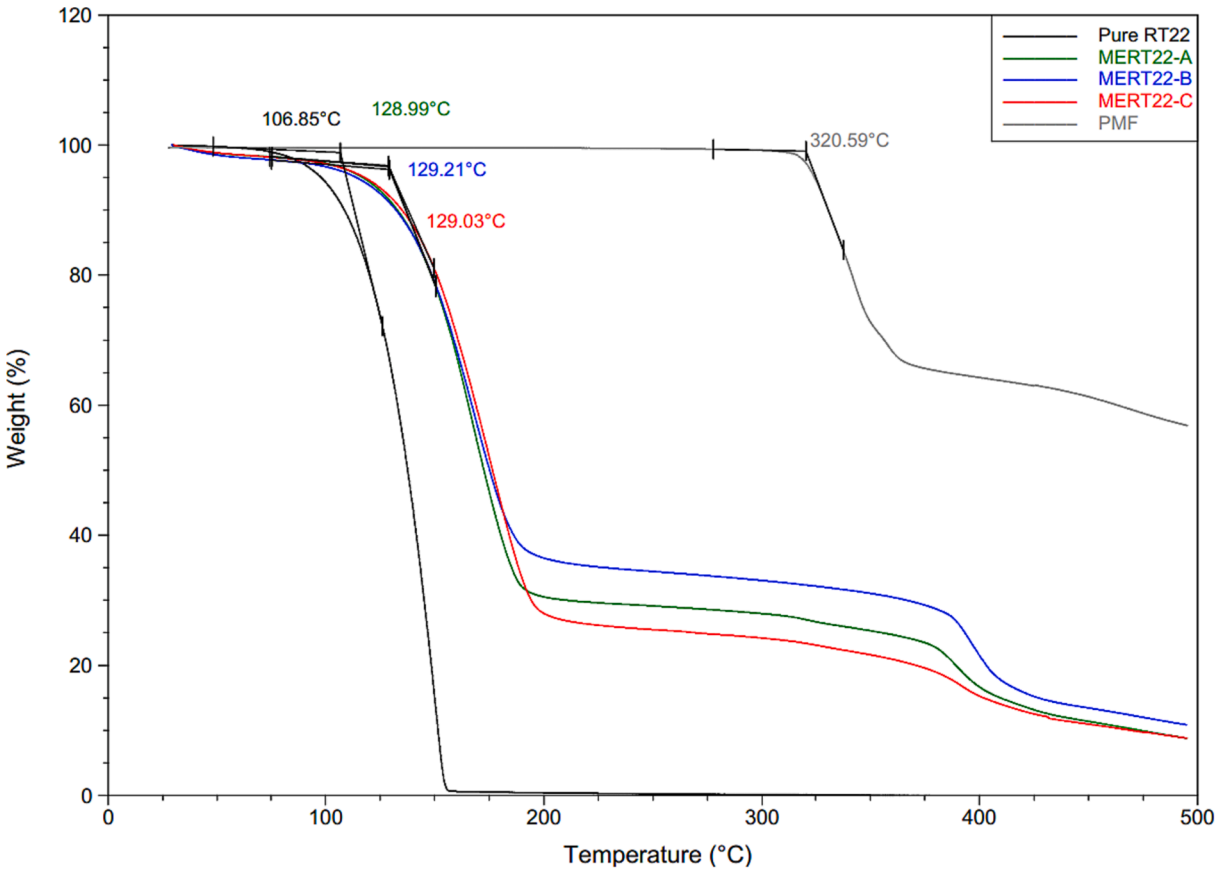

Fig. 10. TG analysis of pure RT22 and MERT22.

profiles of the MERT64 samples are also presented in Fig. 11. The results show that their thermal stabilities were enhanced after encapsulation. Thermal degradation began at 186.09 °C, 200.53 °C, and 190.89 °C for MERT64-A, MERT64-B, and MERT64-C, respectively, in comparison to 184.16 °C for pure RT64. There was however a second stage of degradation above 300 °C, which was attributed to complete decomposition of the PMF shell material at high temperature. As can be seen in Fig. 10, the thermal decomposition of the PMF shell occurred at a temperature of 320.59 °C.

3.2. Characterisation of multiphase change material (MCM)

Based on the overall results in Table 2, samples MERT22-B and MERT64-B were selected as the best combination for the development and characterisation of the MCM which contained 0.125 g of nucleating agent.

3.2.1. Particle size distribution

Fig. 12 displays the range of particle size of MCM sample with a mean diameter of 32.07 μm representing the mean diameter sizes of MERT22-B and MERT64-B. In addition, no particles larger than 200 μm in diameter were identified, which is consistent with the PSD of MERT22-B and MERT64-B depicted in Fig. 4 and Fig. 5, respectively.

3.2.2. Scanning electron microscope (SEM) evaluation

3.2.2.1 Morphology of MCM. The SEM images at various magnifications are exhibited in Fig. 13 to illustrate the impact of shell materials on the size and spherical shape of MCM sample. It can be demonstrated that the majority of particles did retain good level of structural integrity without visible signs of degradation. As can be observed, a large number of particles had a dimension of less than 100 μm, which is in accordance with the results shown in PSD curve.

3.2.2.2 Energy dispersive spectroscopy (EDS). Energy dispersive spectroscopy (EDS) is an auxiliary capability of the JEOL 6490LV SEM apparatus. It was employed for the purpose of acquiring data related to the chemical composition of materials. For the purpose of attaining it, the material underwent irradiation using a high-energy beam in order to induce the emission of X-rays. The property of emitted radiation was subsequently compared to the atomic energy of the corresponding element.

Fig. 14 depicts the EDS result for MCM. Five points analysis were selected randomly for the sample, and the elemental composition was presented both in weight and atomic percentage with a low standard deviation. The presence of signals related to carbon (C), nitrogen (N), and oxygen (O) indicated that these three components dominated the microcapsule shell. Fig. 14 also verifies that the nanosilicon dioxide particles silicon (Si) were effectively included within the capsules as a surfactant. Based on the obtained findings, it is obvious that the appropriate selection of a nanoparticle is crucial in order to mitigate undesired effects, such as the oxidation of metal nanoparticles, which can result in the deterioration of the sample [49].

In addition, a small percentage of chlorine (Cl) was detected on the surface of MCM sample, indicating the presence of a nucleating agent. The other peak in EDS profile was attributed to gold (Au) as the SEM coating material.

Fig. 15 shows the EDS compositional image and map of the MCM sample. The carbon elemental map is shown in red; while nitrogen, oxygen, silicon, and chlorine are respectively represented in orange, green, purple, and blue. These images are consistent with the distribution pattern of the elemental results displayed in Fig. 14.

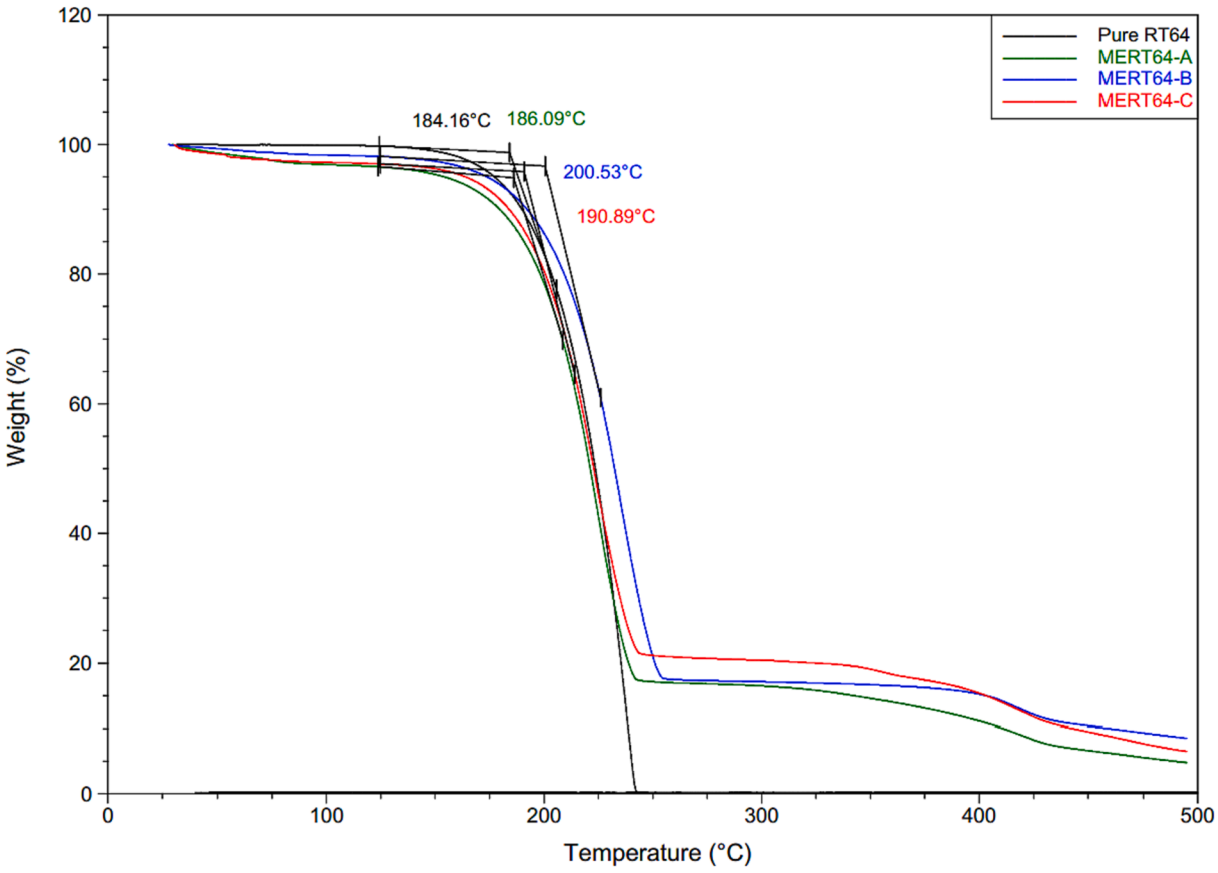

Fig. 11. TG analysis of pure RT64 and MERT64.

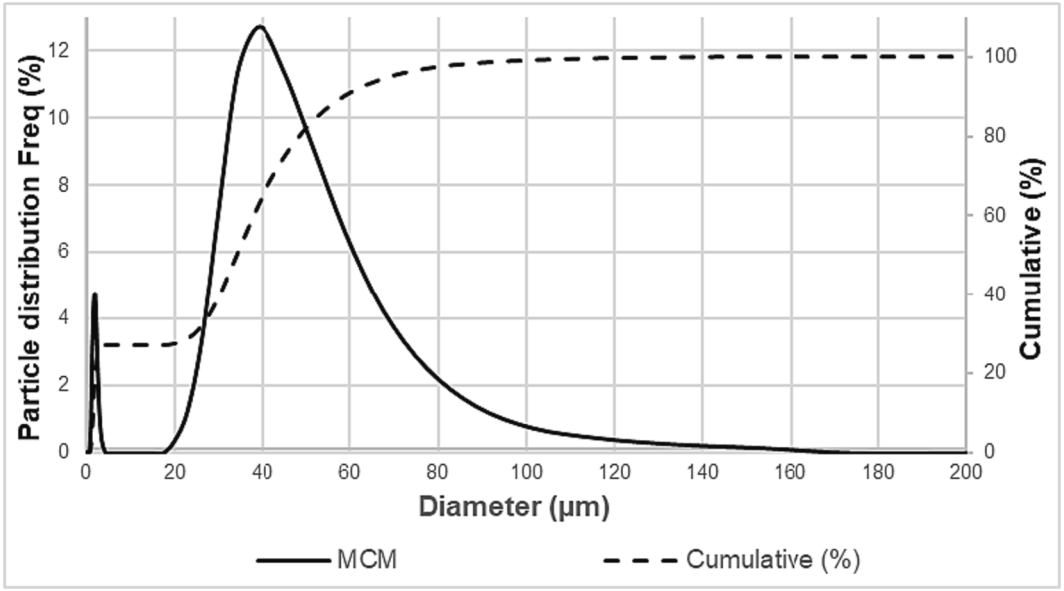

Fig. 12. PSD of MCM sample.

3.2.3. *Energy storage capacity*

The differential thermogram for the MCM is presented in Fig. 16 which shows multiple melting points at 23.01 °C and 56.64 °C with a combined energy storage capacity of 163.17 J/g. This value is slightly less than the theoretical average values of MERT22-B and MERT64-B by about 3.11%. This finding was lower than the result obtained by Su et al. [31], which ranged between 6.34% and 11.41%. In comparison with the average pure PCMs, the heat storage capacity of MCM was about 83.81%. This result was slightly higher than the fabricated MCMs in Ref. [31] with values of 70.69%–76.01% of the average latent heat of pure PCMs. Despite the reduction in the total latent heat capacity, the potential applications of MCMs in buildings appears encouraging given the fact that the fusion energy of commonly used PCMs ranged from 110 to 250 J/g [7].

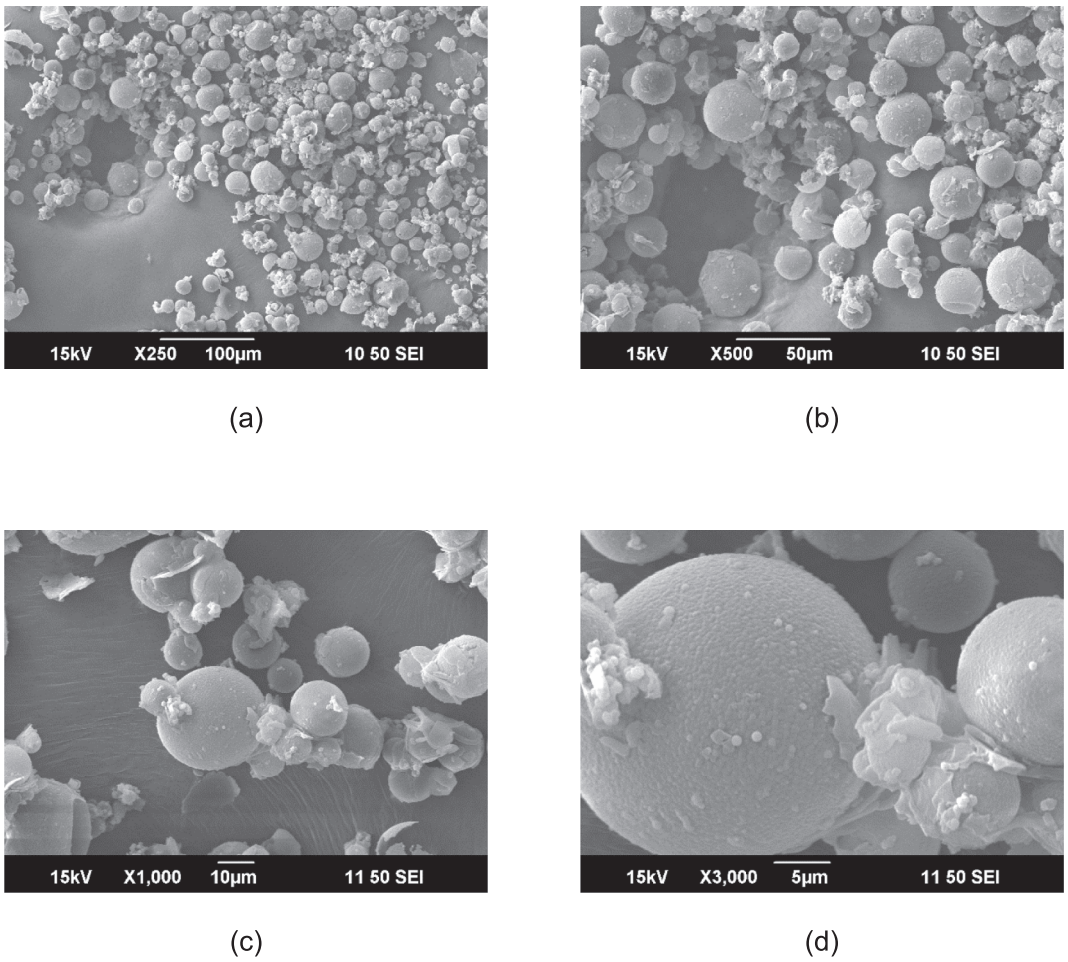

Fig. 13. SEM images of MCM at magnification of (a) X250, (b) X500, (c) X1000, and (d) X3000.

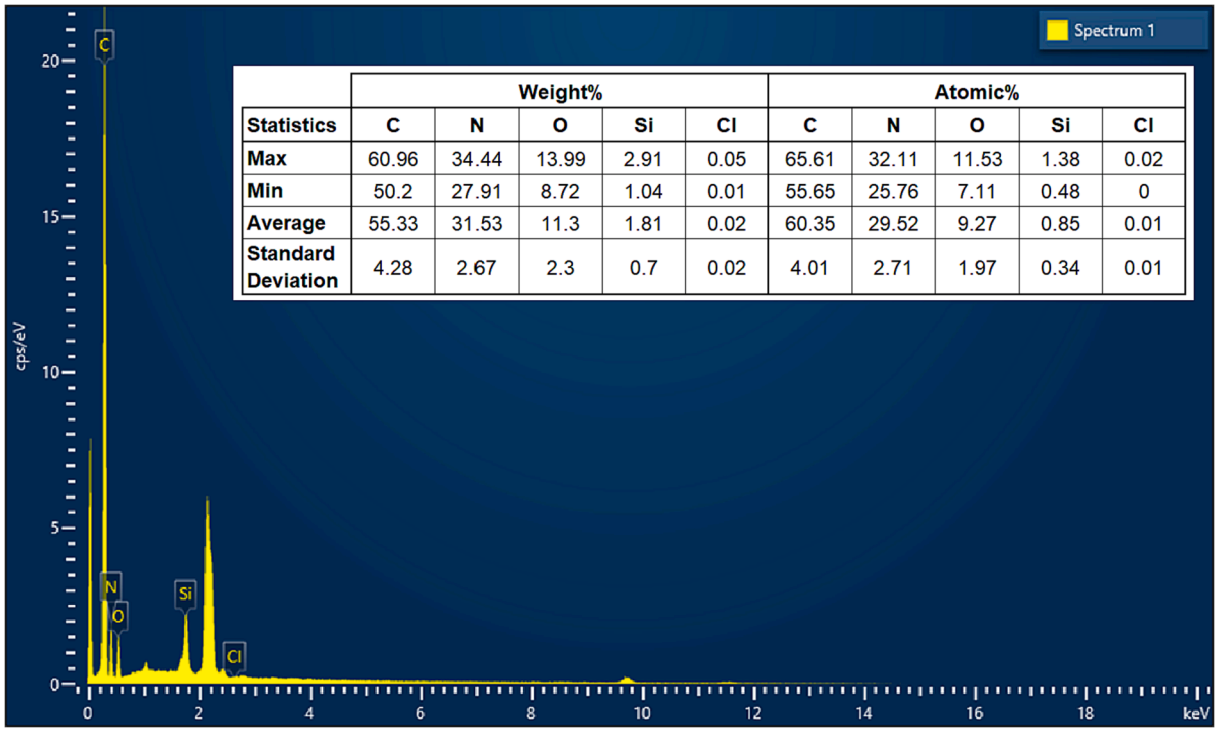

	Weight%					Atomic%				
Statistics	C	N	O	Si	Cl	C	N	O	Si	Cl
Max	60.96	34.44	13.99	2.91	0.05	65.61	32.11	11.53	1.38	0.02
Min	50.2	27.91	8.72	1.04	0.01	55.65	25.76	7.11	0.48	0
Average	55.33	31.53	11.3	1.81	0.02	60.35	29.52	9.27	0.85	0.01
Standard Deviation	4.28	2.67	2.3	0.7	0.02	4.01	2.71	1.97	0.34	0.01

Fig. 14. EDS spectrum of MCM.

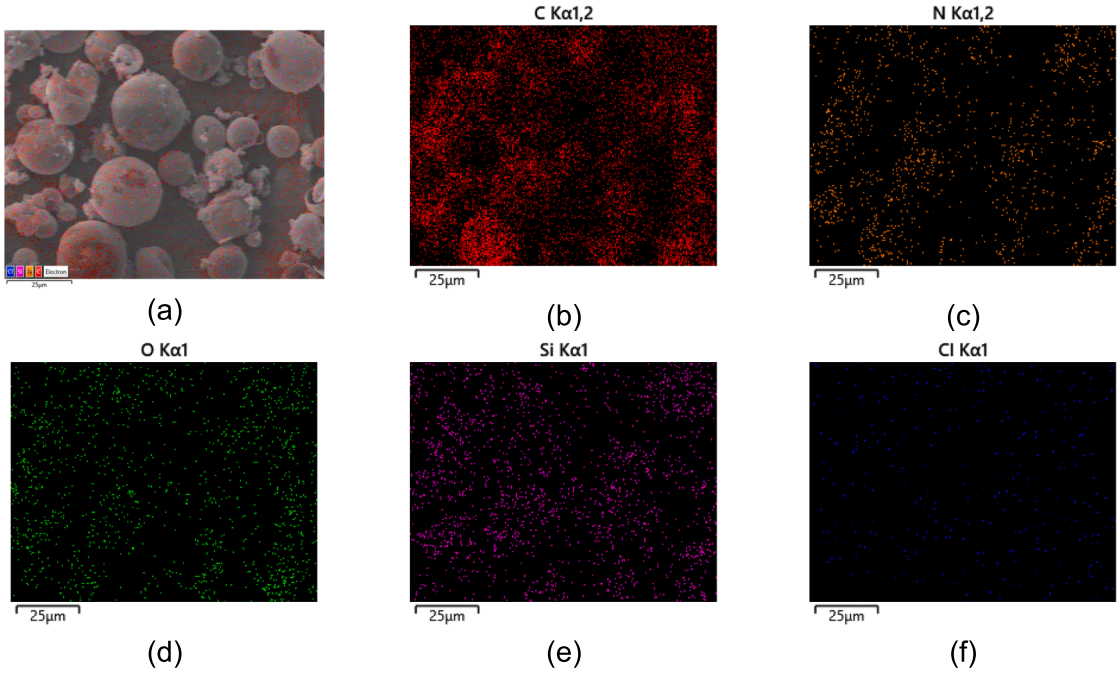

Fig. 15. EDS mapping result of (a) MCM sample for (b) carbon, (c) nitrogen, (d) oxygen, (e) silicon, and (f) chlorine.

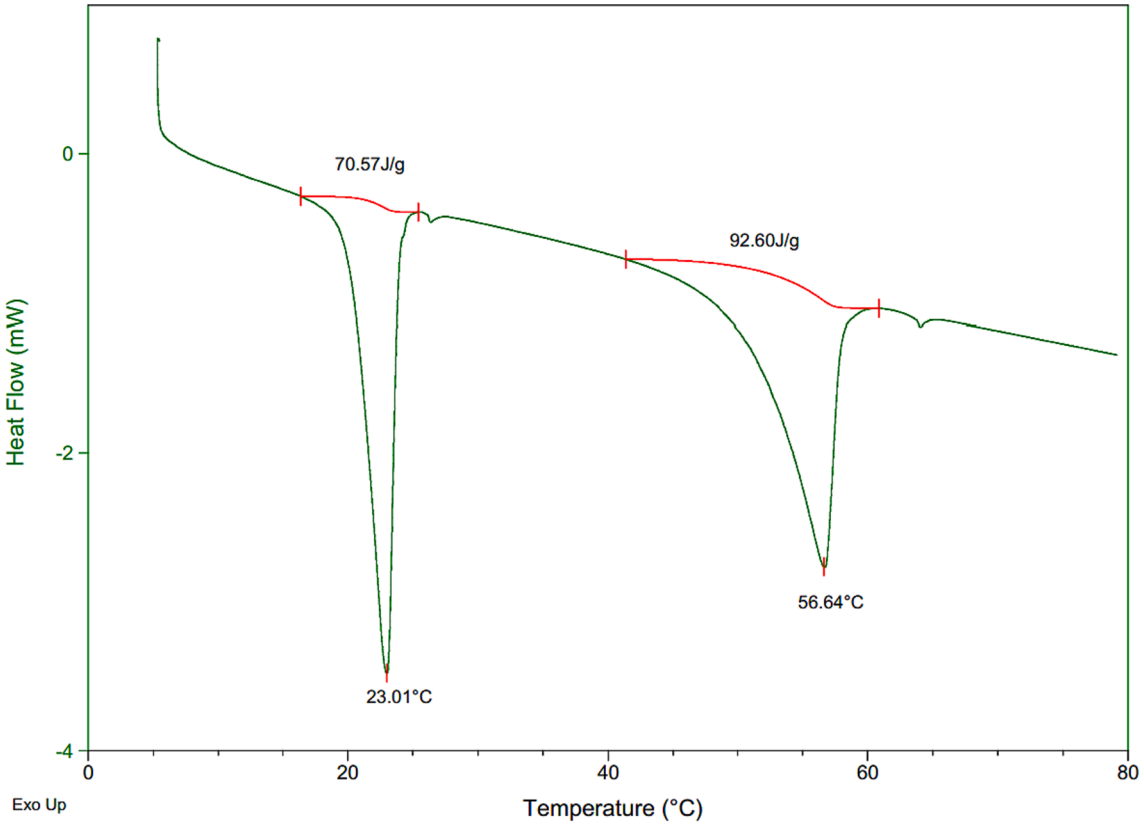

Fig. 16. DSC profile of MCM sample.

3.2.4. Thermal stability

The TGA thermogram of the MCM is shown in Fig. 17. It demonstrates two-step weight loss process with the first weight loss starting at 142.71 °C, which is 35.86 °C above the onset temperature of pristine RT22. Meanwhile, the second weight loss above 300 °C was related to the degradation of PMF shell material.

4. Conclusions

To enhance the encapsulation efficiency and hence the energy

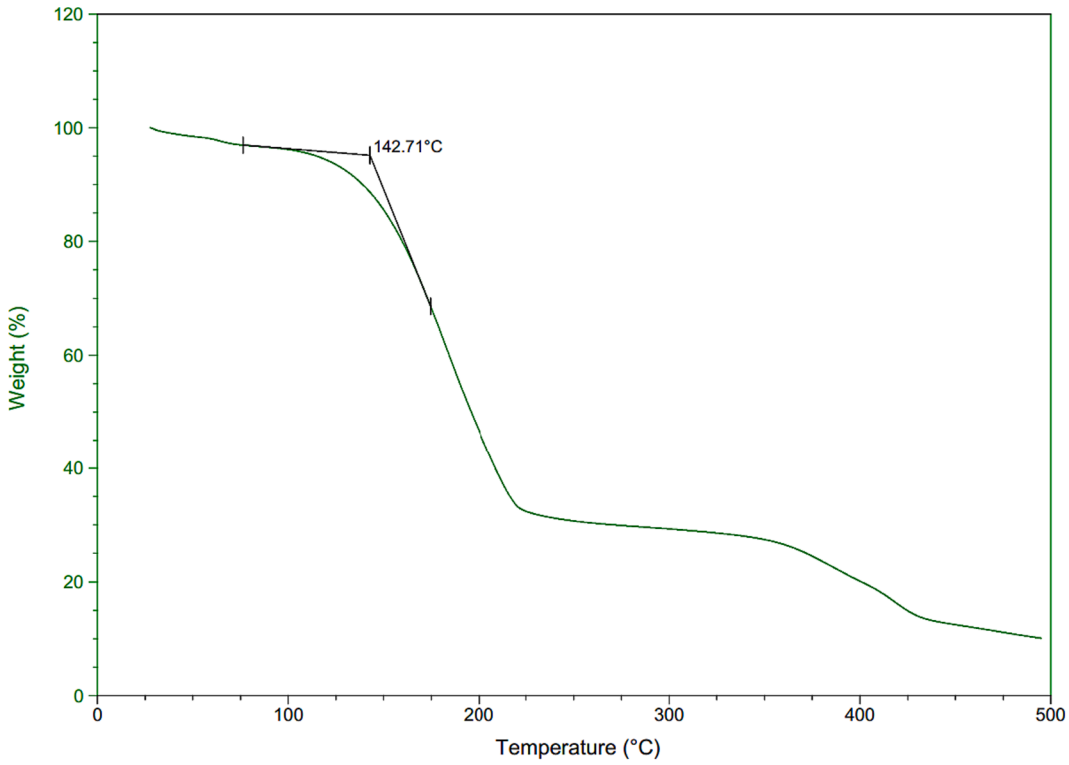

Fig. 17. TG analysis of MCM.

storage capacity, three microencapsulated PCMs (MEPCMs) samples were developed with various proportions of ammonium chloride as a nucleating agent. Analysis of the results showed that samples MERT22-B and MERT64-B were the best combinations for the development of the multiphase change material (MCM) sample which contained 0.125 g of ammonium chloride. The overall analysis showed that an optimum amount of ammonium chloride was critical in achieving high encapsulation efficiencies.The specific findings may therefore be summarised as follows:

a. Samples MERT22-B and MERT64-B achieved the highest encapsulation efficiencies of 90.43% and 84.07%, respectively.
b. The MCM achieved multiple melting points of 23.01 °C and 56.64 °C with combined energy storage capacity of 163.17 J/g which compares favourably with the energy storage capacity of between 110 and 250 J/g for commonly used single phase PCMs.
c. The MCM displayed thermal stability temperature of 142.71 °C which is far higher than any possible environmental conditions for buildings.

Despite the relatively low energy storage capacity, the investigation has demonstrated the positive effect of the nucleating agent on the development of the MCM for both heating and cooling applications in buildings. There is however the need for the thermal response factor to be enhanced upon since it remains as one of the limiting factors of phase change materials.

CRediT authorship contribution statement

Rizal Sinaga: Writing – review & editing, Writing – original draft, Methodology, Investigation, Formal analysis, Data curation, Conceptualization. **Jo Darkwa:** Writing – review & editing, Writing – original draft, Supervision, Project administration, Conceptualization. **Mark Worall:** Writing – review & editing, Writing – original draft, Supervision, Conceptualization. **Weiguang Su:** Writing – review & editing, Supervision, Conceptualization.

Declaration of Competing Interest

The authors declare that they have no known competing financial interests or personal relationships that could have appeared to influence the work reported in this paper.

Data availability

Data will be made available on request.

Acknowledgement

The authors wish to express their gratitude to the Indonesian Ministry of Education and Culture; for funding this research through Beasiswa Pendidikan Pascasarjana Luar Negeri (BPPLN). The authors also would like to thank the Shandong Province Department of Education (Sub-Title: Innovative Research Team of Advanced Energy Equipment). The authors would like to gratefully acknowledge the Nanoscale and Microscale Research Centre (nmRC) at the University of Nottingham for SEM facility. The authors also thankfully acknowledge the Howdle Group at the School of Chemistry, University of Nottingham, in particular Vincenzo Taresco and Joachim Lentz for their technical assistance in TGA and DSC test. The authors also would like to thank the UK EPSRC Grant (No. EP/V041452/1).

References

[1] M.M. Bhatti, K. Vafai, S.I. Abdelsalam, The role of nanofluids in renewable energy engineering, Nanomaterials 13 (2023) 2–5, https://doi.org/10.3390/nano13192671.
[2] H. Zhang, Q. Dong, J. Lu, Y. Tang, W. Bi, Y. Gao, et al., Modified sodium acetate trihydrate/expanded perlite composite phase change material encapsulated by epoxy resin for radiant floor heating, J. Energy Storage 65 (2023), 107374, https://doi.org/10.1016/j.est.2023.107374.
[3] A. Ismail, J. Zhou, A. Aday, I. Davidoff, A. Odukomaiya, J. Wang, Microencapsulation of bio-based phase change materials with silica coated

inorganic shell for thermal energy storage, J. Build. Eng. 67 (2023), 105981, https://doi.org/10.1016/j.jobe.2023.105981.
[4] Y. Konuklu, M. Ostry, H.O. Paksoy, P. Charvat, Review on using microencapsulated phase change materials (PCM) in building applications, Energ. Buildings 106 (2015) 134–155, https://doi.org/10.1016/j.enbuild.2015.07.019.
[5] T.A. Mukram, J. Daniel, A review of novel methods and current developments of phase change materials in the building walls for cooling applications, Sustain. Energy Technol. Assessments 49 (2022), 101709, https://doi.org/10.1016/j.seta.2021.101709.
[6] R. Sinaga, J. Darkwa, S.A. Omer, M. Worall, The microencapsulation, thermal enhancement, and applications of medium and high-melting temperature phase change materials: A review, Int. J. Energy Res. (2022), https://doi.org/10.1002/er.7860.
[7] N. Soares, T. Matias, L. Durães, P.N. Simões, J.J. Costa, Thermophysical characterization of paraffin-based PCMs for low temperature thermal energy storage applications for buildings, Energy (2023) 269, https://doi.org/10.1016/j.energy.2023.126745.
[8] J. Darkwa, T. Zhou, Enhanced laminated composite phase change material for energy storage, Energy Convers. Manag. 52 (2011) 810–815, https://doi.org/10.1016/j.enconman.2010.08.006.
[9] T. Zhou, J. Darkwa, G. Kokogiannakis, Thermal evaluation of laminated composite phase change material gypsum board under dynamic conditions, Renew. Energy 78 (2015) 448–456, https://doi.org/10.1016/j.renene.2015.01.025.
[10] J. Bohórquez-Órdenes, A. Tapia-Calderón, D.A. Vasco, O. Estuardo-Flores, A. N. Haddad, Methodology to reduce cooling energy consumption by incorporating PCM envelopes: a case study of a dwelling in Chile, Build. Environ. (2021) 206, https://doi.org/10.1016/j.buildenv.2021.108373.
[11] G. Nurlybekova, S.A. Memon, I. Adilkhanova, Quantitative evaluation of the thermal and energy performance of the PCM integrated building in the subtropical climate zone for current and future climate scenario, Energy 219 (2021), 119587, https://doi.org/10.1016/j.energy.2020.119587.
[12] S. Wijesuriya, P.C. Tabares-Velasco, Empirical validation and comparison of methodologies to simulate micro and macro-encapsulated PCMs in the building envelope, Appl. Therm. Eng. 188 (2021), 116646, https://doi.org/10.1016/j.applthermaleng.2021.116646.
[13] M.A. Fazilati, A.A. Alemrajabi, Phase change material for enhancing solar water heater, an experimental approach, Energy Convers Manag 71 (2013) 138–145, https://doi.org/10.1016/j.enconman.2013.03.034.
[14] M.K.A. Sharif, A.A. Al-Abidi, S. Mat, K. Sopian, M.H. Ruslan, M.Y. Sulaiman, et al., Review of the application of phase change material for heating and domestic hot water systems, Renew. Sustain. Energy Rev. 42 (2015) 557–568, https://doi.org/10.1016/j.rser.2014.09.034.
[15] A. Najafian, F. Haghighat, A. Moreau, Integration of PCM in domestic hot water tanks: Optimization for shifting peak demand, Energ. Buildings 106 (2015) 59–64, https://doi.org/10.1016/j.enbuild.2015.05.036.
[16] R.E. Murray, D. Groulx, Experimental study of the phase change and energy characteristics inside a cylindrical latent heat energy storage system: Part 1 consecutive charging and discharging, Renew. Energy 62 (2014) 571–581, https://doi.org/10.1016/j.renene.2013.08.007.
[17] M. Delgado, A. Lázaro, J. Mazo, C. Peñalosa, P. Dolado, B. Zalba, Experimental analysis of a low cost phase change material emulsion for its use as thermal storage system, Energy Convers. Manag. 106 (2015) 201–212, https://doi.org/10.1016/j.enconman.2015.09.033.
[18] H. Bo, E.M. Gustafsson, F. Setterwall, Tetradecane and hexadecane binary mixtures as phase change materials (PCMs) for cool storage in district cooling systems, Energy 24 (1999) 1015–1028, https://doi.org/10.1016/S0360-5442(99)00055-9.
[19] Y. Ma, Q. Xie, X. Wang, Investigations on thermal properties of microencapsulated phase-change materials with different acrylate-based copolymer shells as thermal insulation materials, J. Appl. Polym. Sci. 136 (2019) 1–12, https://doi.org/10.1002/app.47777.
[20] M. Li, Z. Wu, H. Kao, Study on preparation and thermal properties of binary fatty acid/diatomite shape-stabilized phase change materials, Sol. Energy Mater. Sol. Cells 95 (2011) 2412–2416, https://doi.org/10.1016/j.solmat.2011.04.017.
[21] K.K. Kadyrzhanov, D.I. Shlimas, A.L. Kozlovskiy, M.V. Zdorovets, Research of the shielding effect and radiation resistance of composite CuBi2O4 films as well as their practical applications, J. Mater. Sci. Mater. Electron. 31 (2020) 11729–11740, https://doi.org/10.1007/s10854-020-03724-w.
[22] A.L. Kozlovskiy, M.V. Zdorovets, Synthesis, structural, strength and corrosion properties of thin films of the type CuX (X = Bi, Mg, Ni), J. Mater. Sci. Mater. Electron. 30 (2019) 11819–11832, https://doi.org/10.1007/s10854-019-01556-x.
[23] M.V. Zdorovets, A.L. Kozlovskiy, D.I. Shlimas, D.B. Borgekov, Phase transformations in FeCo – Fe2CoO4/Co3O4-spinel nanostructures as a result of thermal annealing and their practical application, J. Mater. Sci. Mater. Electron. 32 (2021) 16694–16705, https://doi.org/10.1007/s10854-021-06226-5.
[24] M.I. Panasyuk, T.I. Zubar, T.I. Usovich, D.I. Tishkevich, O.D. Kanafyev, V. A. Fedkin, et al., Mechanism of bubbles formation and anomalous phase separation in the CoNiP system, Sci. Rep. 13 (2023) 1–7, https://doi.org/10.1038/s41598-023-33146-7.
[25] A. Ricklefs, A.M. Thiele, G. Falzone, G. Sant, L. Pilon, Thermal conductivity of cementitious composites containing microencapsulated phase change materials, Int. J. Heat Mass Transf. 104 (2017) 71–82, https://doi.org/10.1016/j.ijheatmasstransfer.2016.08.013.
[26] A.M. Borreguero, M. Carmona, M.L. Sanchez, J.L. Valverde, J.F. Rodriguez, Improvement of the thermal behaviour of gypsum blocks by the incorporation of microcapsules containing PCMS obtained by suspension polymerization with an optimal core/coating mass ratio, Appl. Therm. Eng. 30 (2010) 1164–1169, https://doi.org/10.1016/j.applthermaleng.2010.01.032.
[27] N. Rosa, J. Costa, A. Lopes, T. Matias, P. Simões, L. Durães, Validation of different numerical models with benchmark 2 experiments for modelling microencapsulated-PCM-based applications for buildings 159 (2021), doi: 10.1016/j.ijthermalsci.2020.106565.
[28] M. Graham, J.A. Coca-Clemente, E. Shchukina, D. Shchukin, Nanoencapsulated crystallohydrate mixtures for advanced thermal energy storage, J. Mater. Chem. A 5 (2017) 13683–13691, https://doi.org/10.1039/c7ta02494k.
[29] Y. Yang, R. Xia, J. Zhao, L. Shang, Y. Liu, H. Guo, Preparation and thermal properties of microencapsulated polyurethane and double-component poly (ethylene glycol) as phase change material for thermal energy storage by interfacial polymerization, Energy Fuel 34 (2020) 1024–1032, https://doi.org/10.1021/acs.energyfuels.9b03435.
[30] J. Darkwa, W. Su, Multiphase change materials for energy storage application in buildings, 14th Int. Energy Convers. Eng. Conf. 2016 (2016), https://doi.org/10.2514/6.2016-4602.
[31] W. Su, J. Darkwa, T. Zhou, D. Du, G. Kokogiannakis, Y. Li, et al., Development of composite microencapsulated phase change materials for multi-temperature thermal energy storage, Crystals (2023) 13, https://doi.org/10.3390/cryst13081167.
[32] K. Mai, K. Wang, H. Zeng, Multiple melting behavior of nucleated polypropylene, J. Appl. Polym. Sci. 88 (2003) 1608–1611, https://doi.org/10.1002/app.11652.
[33] J.L. Zeng, L. Zhou, Y.F. Zhang, S.L. Sun, Y.H. Chen, L. Shu, et al., Effects of some nucleating agents on the supercooling of erythritol to be applied as phase change material, J. Therm. Anal. Calorim. 129 (2017) 1291–1299, https://doi.org/10.1007/s10973-017-6296-2.
[34] J.L. Alvarado, C. Marsh, C. Sohn, M. Vilceus, V. Hock, G. Phetteplace, et al., Characterization of supercooling suppression of microencapsulated phase change material by using DSC, J. Therm. Anal. Calorim. 86 (2006) 505–509, https://doi.org/10.1007/s10973-005-7430-0.
[35] A.L. Kozlovskiy, M.V. Zdorovets, Study of hydrogenation processes in radiation-resistant nitride ceramics, J. Mater. Sci. Mater. Electron. 31 (2020) 11227–11237, https://doi.org/10.1007/s10854-020-03671-6.
[36] S. Lashgari, A.R. Mahdavian, H. Arabi, V. Ambrogi, V. Marturano, Preparation of acrylic PCM microcapsules with dual responsivity to temperature and magnetic field changes, Eur. Polym. J. 101 (2018) 18–28, https://doi.org/10.1016/j.eurpolymj.2018.02.011.
[37] H. Zhang, X. Wang, Fabrication and performances of microencapsulated phase change materials based on n-octadecane core and resorcinol-modified melamine-formaldehyde shell, Colloids Surf. A Physicochem. Eng. Asp. 332 (2009) 129–138, https://doi.org/10.1016/j.colsurfa.2008.09.013.
[38] W. Su, J. Darkwa, G. Kokogiannakis, Nanosilicon dioxide hydrosol as surfactant for preparation of microencapsulated phase change materials for thermal energy storage in buildings, Int. J. Low-Carbon Technol. 13 (2018) 301–310, https://doi.org/10.1093/ijlct/cty032.
[39] W. Su, Y. Li, T. Zhou, J. Darkwa, G. Kokogiannakis, Z. Li, Microencapsulation of paraffin with poly (urea methacrylate) shell for solar water heater, Energies (2019) 12, https://doi.org/10.3390/en12183406.
[40] A. Khezri, M. Sahebi, M. Mohammadi, Fabrication and Thermal properties of graphene nanoplatelet-enhanced phase change materials based on paraffin encapsulated by melamine–formaldehyde, J. Therm. Anal. Calorim. 147 (2022) 7683–7691, https://doi.org/10.1007/s10973-021-11085-7.
[41] G.V.N. Trivedi, R. Parameshwaran, Cryogenic conditioning of microencapsulated phase change material for thermal energy storage, Sci. Rep. 10 (2020) 1–11, https://doi.org/10.1038/s41598-020-75494-8.
[42] W. Li, J. Wang, X. Wang, S. Wu, X. Zhang, Effects of ammonium chloride and heat treatment on residual formaldehyde contents of melamine-formaldehyde microcapsules, Colloid Polym. Sci. 285 (2007) 1691–1697, https://doi.org/10.1007/s00396-007-1744-3.
[43] C. Fan, X. Zhou, Influence of operating conditions on the surface morphology of microcapsules prepared by in situ polymerization, Colloids Surf. A Physicochem. Eng. Asp. 363 (2010) 49–55, https://doi.org/10.1016/j.colsurfa.2010.04.012.
[44] J. Tang, C. Fan, Q. Lin, X. Zhou, Smooth, stable and optically transparent microcapsules prepared by one-step method using sodium carboxymethyl cellulose as protective colloid, Colloids Surf. A Physicochem. Eng. Asp. 459 (2014) 65–73, https://doi.org/10.1016/j.colsurfa.2014.06.044.
[45] A. Sari, C. Alkan, A. Altintaş, Preparation, characterization and latent heat thermal energy storage properties of micro-nanoencapsulated fatty acids by polystyrene shell, Appl. Therm. Eng. 73 (2014) 1160–1168, https://doi.org/10.1016/j.applthermaleng.2014.09.005.
[46] V.E. Tsvetkov, O.P. Machneva, Impregnating compositions for lamination of wood materials, Polym. Sci. – Ser. D 13 (2020) 31–33, https://doi.org/10.1134/S1995421220010232.
[47] F. He, G. Song, X. He, C. Sui, M. Li, Structural and phase change characteristics of inorganic microencapsulated core/shell Al–Si/Al2O3 micro-particles during thermal cycling, Ceram. Int. 41 (2015) 10689–10696, https://doi.org/10.1016/j.ceramint.2015.05.001.
[48] C. Xin, Y. Tian, Y. Wang, X. Huang, Effect of curing temperature on the performance of microencapsulated low melting point paraffin using urea-formaldehyde resin as a shell, Text. Res. J. 84 (2014) 831–839, https://doi.org/10.1177/0040517513507367.
[49] A. Kozlovskiy, K. Egizbek, M.V. Zdorovets, M. Ibragimova, A. Shumskaya, A. Rogachev, et al., Evaluation of the Efficiency of Detection and Capture of Manganese in Aqueous Solutions of FeCeOx Nanocomposites Doped with Nb2O5, Sens. Lett. 20 (2020) 4851.